Complete polarization and phase control for focus-shaping in high-NA microscopy

F. Kenny,[1,*] **D. Lara,**[2] **O. G. Rodríguez-Herrera,**[3] **and C. Dainty**[1]

[1]*Applied Optics, School of Physics, National University of Ireland, Galway, University Rd., Galway, Ireland*
[2]*The Blackett Laboratory, Imperial College London, SW7 2BW, UK*
[3]*College of Optical Sciences,University of Arizona, Tucson, AZ 85721, USA*
**f.kenny1@nuigalway.ie*

Abstract: We show that, in order to attain complete polarization control across a beam, two spatially resolved variable retardations need to be introduced to the light beam. The orientation of the fast axes of the retarders must be linearly independent on the Poincaré sphere if a fixed starting polarization state is used, and one of the retardations requires a range of 2π. We also present an experimental system capable of implementing this concept using two passes on spatial light modulators (SLMs). A third SLM pass can be added to control the absolute phase of the beam. Control of the spatial polarization and phase distribution of a beam has applications in high-NA microscopy, where these properties can be used to shape the focal field in three dimensions. We present some examples of such fields, both theoretically calculated using McCutchen's method and experimentally observed.

OCIS codes: (260.5430) Polarization; (110.0180) Microscopy; (180.6900) Three-dimensional microscopy; (070.6120) Spatial light modulators; (120.5060) Phase modulation.

References and links

1. B. Richards and E. Wolf, "Electromagnetic diffraction in optical systems II. structure of the image field in an aplanatic system," Proc. R. Soc. London Ser. A **253**, 358–379 (1959).
2. R. Dorn, S. Quabis, and G. Leuchs, "Sharper focus for a radially polarized light beam," Phys. Rev. Lett. **91**, 233901 (2003).
3. Q. Zhan, "Trapping metallic Rayleigh particles with radial polarization," Opt. Express **12**, 3377–3382 (2004).
4. V. G. Niziev and A. V. Nesterov, "Influence of beam polarization on laser cutting efficiency," J. Phys. D: Appl. Phys. **32**, 1455–1461 (1999).
5. C. J. R. Sheppard and A. Choudhury, "Annular pupils, radial polarization, and superresolution," Appl. Opt. **43**, 4322–4327 (2004).
6. T. Klar, E. Engel, and S. W. Hell, "Breaking Abbe's diffraction limit in fluorescence microscopy with stimulated emission depletion beams of various shapes," Phys. Rev. E **64**, 066613 (2001).
7. K. S. Youngworth and T. G. Brown, "Focusing of high numerical aperture cylindrical-vector beams," Opt. Express **7**, 1543–1545 (2000).
8. D. P. Biss and T. G. Brown, "Cylindrical vector beam focusing through a dielectric interface," Opt. Express **9**, 490–497 (2001).
9. A. K. Spilman and T. J. Brown, "Stress birefringent, space-variant wave plates for vortex illumination," Appl. Opt. **46**, 61–66 (2007).
10. T. Grosjean, D. Courjon, and M. Spajer, "An all-fiber device for generating radially and other polarized light beams," Opt. Commun. **203**, 1–5 (2002).
11. S. C. Tidwell, D. H. Ford, and W. D. Kimura, "Generating radially polarized beams interferometrically," Appl. Opt. **29**, 2234–2239 (1990).

#167770 - $15.00 USD Received 1 May 2012; revised 28 May 2012; accepted 29 May 2012; published 8 Jun 2012

12. S. N. Khonina and I. Golub, "Optimization of focusing of linearly polarized light," Opt. Lett. **36**, 352–354 (2011).
13. W. S. Shurcliff and S. S. Ballard, *Polarized Light* (D. Van Nostrand Company Inc., 1964)
14. D. Lara and C. Dainty, "Double-pass axially resolved confocal Mueller matrix imaging polarimetry," Opt. Lett. **30**, 2879–2781 (2005).
15. Z. Zhuang, S.-W. Suh, and J. S. Patel, "Polarization controller using nematic liquid crystals," Opt. Lett. **24**, 694–696 (1999)
16. I. Moreno, J. A. Davis, T. M. Hernandez, D. M. Cottrell, and D. Sand, "Complete polarization control of light from a liquid crystal spatial light modulator," Opt. Express **20**, 364–376 (2011).
17. H. Chen, J. Hao, B.-f. Zhang, J. Xu, J. Ding, and H.-t. Wang, "Generation of vector beam with space-variant distribution of both polarization and phase," Opt. Lett. **36**, 3179–3181 (2011).
18. D. H. Goldstein, *Polarized Light*, 3rd ed. (CRC Press, 2011).
19. O. G. Rodríguez-Herrera, D. Lara, and C. Dainty, "Far-field polarization-based sensitivity to sub-resolution displacements of a sub-resolution scatterer in tightly focused fields," Opt. Express **18**, 5609–5628 (2010).
20. O. G. Rodríguez-Herrera, D. Lara, K. Bliokh, E. Ostravskaya, and C. Dainty, "Optical nanoprobing via spin-orbit interaction of light," Phys. Rev. Lett. **104**, 253601 (2010).
21. E. Compain, S. Poirier, and B. Drevillon, "General and self-consistent method for the calibration of polarization modulators, polarimeters and Mueller-matrix ellipsometers," Appl. Opt. **38**, 3490–3502 (1999).
22. D. Lara and C. Dainty, "Axially resolved complete Mueller matrix confocal microscopy," Appl. Opt. **45**, 1917–1930 (2006).
23. J. L. Pezzaniti and R. A. Chipman, "Linear polarization uniformity measurements taken with an imaging polarimeter," Opt. Eng. **34**, 1569–1573 (1995).
24. C. W. McCutchen, "Generalized aperture and the three-dimensional diffraction image," J. Opt. Soc. Am. **54**, 240–242 (1964).
25. C. W. McCutchen, "Generalized aperture and the three-dimensional diffraction image: erratum," J. Opt. Soc. Am. A **19**, 1721–1721 (2002).
26. J. Lin, O. G. Rodríguez-Herrera, F. Kenny, D. Lara, and C. Dainty, "Fast vectorial calculation of the volumetric focused field distribution by using a three-dimensional Fourier transform," Opt. Express **20**, 1060–1069 (2012).
27. I. Iglesias and B. Vohnsen, "Polarization structuring for focal volume shaping in high-resolution microscopy," Opt. Commun. **271**, 40–47 (2007).
28. Q. Zhan, "Cylindrical vector beams: from mathematical concepts to applications," Adv. Opt. Photon. **1**, 1–57 (2009).
29. M. Beresna, M. Gecevičius, P. G. Kazansky, and T. Gertus, "Radially polarized optical vortex converter created by femtosecond laser nanostructuring of glass," Appl. Phys. Lett. **98**, 201101 (2011).
30. J. Braat, P. Dirksen, and A. J. E. M. Janssen, "Assessment of an extended Nijboer–Zernike approach for the computation of optical point-spread functions ," J. Opt. Soc. Am. A **19**, 858–870 (2004).
31. M. Born and E. Wolf, *Principles of Optics* (Pergamon Press, 1980).

1. Introduction

The focal field of a high numerical aperture lens is strongly dependent on the polarization state in the pupil before focusing. This was first explained by Richards & Wolf [1] using vectorial diffraction integrals, who showed, as an example, that focusing a linearly polarized distribution in the pupil of the lens results in an elongated, elliptical focal field distribution. It was later found that a radially polarized distribution in the pupil results in a focal spot sharper than the Airy disc [2]. This property has found uses in many applications, such as optical trapping [3], laser cutting [4], and improved resolution in imaging [5]. Uses for the doughnut-shaped focal field arising from focusing an azimuthally polarized distribution were also found, for example in the depletion step of STED microscopy [6].

Azimuthal and radial polarization distributions are two examples of cylindrical vector beams [7,8]. A cylindrical vector beam is essentially a realization of a phase vortex, as shown in Fig. 1, which is the result of a localized rotation of the coordinate system that follows the azimuthal angle of the polar cylindrical coordinate system. Resolving a radial polarization distribution into its x- and y-components reveals this dependence of cylindrical vector beams on the absolute phase, as shown in Fig. 2. We could use a polar coordinate system, resolving the field into its radial and azimuthal components instead of x- and y-. In this case only two parameters would be needed to describe a cylindrical vector beam instead of three when using cartesian

#167770 - $15.00 USD Received 1 May 2012; revised 28 May 2012; accepted 29 May 2012; published 8 Jun 2012

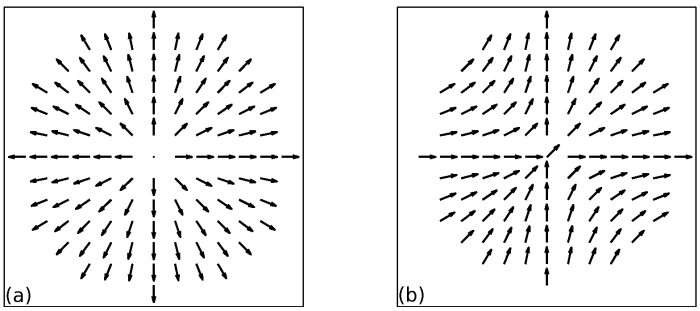

Fig. 1. Any cylindrically polarized vector beam includes a phase vortex. (a) Includes a vortex in its absolute phase, while (b) has a flat phase distribution. (b) Was calculated by resolving (a) into its *x*- and *y*-components, and removing the phase discontinuity present in each of the components. Differences in the polarization, as well as the absolute phase, arise out of this flattening, for example in the upper left quadrant of the pupil.

coordinates. This is because a polar coordinate system intrinsically incorporates a phase vortex of topological charge 1 that is characteristic of cylindrical vector beams. In the laboratory, however, this type of beam cannot be generated without a degree of control of the absolute phase as a function of the position on the pupil. Locally, within the pupil, the orientations of the fast and slow axes of variable retarders (e.g. SLMs) are often fixed. Furthermore, the state of polarization of common light sources is also fixed and homogenous across the waist of the beam. Other configurations are possible, for example using spatially variant waveplates [9], fibers [10], or interferometric methods [11], but, in general, variable control of three parameters at each locus on the pupil is necessary for complete polarization control.

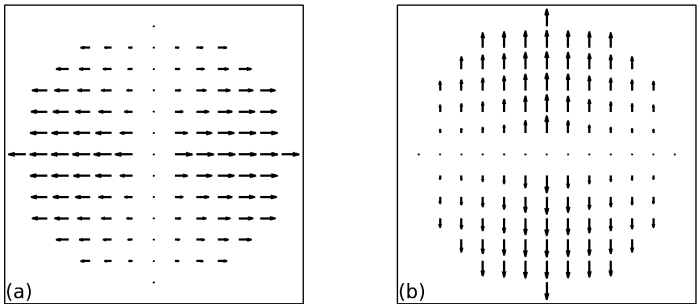

Fig. 2. Resolving a radially polarized beam into its *x*- and *y*- components reveals the phase discontinuity at the centre more clearly; (a) and (b) show the *x*- and *y*-components of a radial distribution, which was previously shown in Fig. 1(a).

Additional absolute phase control as well as spatial polarization control is necessary to have full control of the longitudinal component of the focused field in the laboratory. Some focal field distributions cannot be attained with polarization control alone. For example, a collimated beam with homogeneous polarization cannot be converted to produce a longitudinal component of the focused field on axis unless the absolute phase is effectively manipulated [12].

In Section 2 we use the Poincaré sphere representation to discuss what it means to attain complete polarization control. This is supported using analysis in the Jones formalism. An experimental system capable of implementing the concepts is described in Section 3, along with numerical and experimental results of fields that can be generated when these polarization dis-

#167770 - $15.00 USD Received 1 May 2012; revised 28 May 2012; accepted 29 May 2012; published 8 Jun 2012

tributions are tightly focused. Section 4 builds on the experimental system shown in Section 3 by adding the ability to control the absolute phase, along with the polarization, of the distribution. Finally, before the discussion, we show a further example of a polarization distribution suitable for high-NA optical nano-probing, which was defined using Zernike polynomials.

2. Theory

The Poincaré sphere is a three-dimensional representation of the Stokes parameters. Every possible pure polarization state can be represented as a point on its surface [13]. The effect of a linear retarder on any polarization is suitably depicted as a rotation on the Poincaré sphere; the axis of this rotation is defined by the orientation of the fast axis of the retarder. Mueller analysis is used below to see this algebraically.

The Mueller matrix of a retarder of retardance δ and with its fast axis at 0° is

$$\mathbf{M}_{ret}(\delta, 0^\circ) = \begin{pmatrix} 1 & 0 & 0 & 0 \\ 0 & 1 & 0 & 0 \\ 0 & 0 & \cos\delta & \sin\delta \\ 0 & 0 & -\sin\delta & \cos\delta \end{pmatrix}. \tag{1}$$

In order to convert this into the Mueller matrix of a retarder with fast axis at an angle of 45°, we must simply compute the following matrix product

$$\mathbf{M}_{ret}(\delta, 45^\circ) = \mathbf{M}_{rot}(45^\circ) \cdot \mathbf{M}_{ret}(\delta, 0^\circ) \cdot \mathbf{M}_{rot}(-45^\circ), \tag{2}$$

where $\mathbf{M}_{rot}(\theta)$ is the Mueller matrix representation for a rotation around the optical axis of an angle θ:

$$\mathbf{M}_{rot}(\theta) = \begin{pmatrix} 1 & 0 & 0 & 0 \\ 0 & \cos 2\theta & -\sin 2\theta & 0 \\ 0 & \sin 2\theta & \cos 2\theta & 0 \\ 0 & 0 & 0 & 1 \end{pmatrix}. \tag{3}$$

We now consider the effect of a retarder, such as the one described by Eq. (2), on an incident beam which is linearly polarized in the horizontal direction. Its Stokes vector is

$$\mathbf{s}_{in} = \begin{pmatrix} 1 \\ 1 \\ 0 \\ 0 \end{pmatrix}. \tag{4}$$

The Stokes vector of the beam after the retarder at 45° is

$$\mathbf{s}_{out} = \mathbf{M}_{ret}(\delta, 45^\circ) \cdot \mathbf{s}_{in}. \tag{5}$$

Computation of Eq. (5), using Eqs. (4) and (2), reveals that the state of polarization of the output beam is the result of a rotation of angle δ on the surface of the sphere:

$$\mathbf{s}_{out} = \begin{pmatrix} 1 \\ \cos\delta \\ 0 \\ \sin\delta \end{pmatrix}. \tag{6}$$

In our example, the starting point of the rotation is linear horizontally polarized light (see point H in Fig. 3), and the rotation is left-handed (clockwise) around the 45° axis. A familiar example of this is when $\delta = \pi/2$, which makes the retarder in Eq. (5) a quarter waveplate at

#167770 - $15.00 USD Received 1 May 2012; revised 28 May 2012; accepted 29 May 2012; published 8 Jun 2012

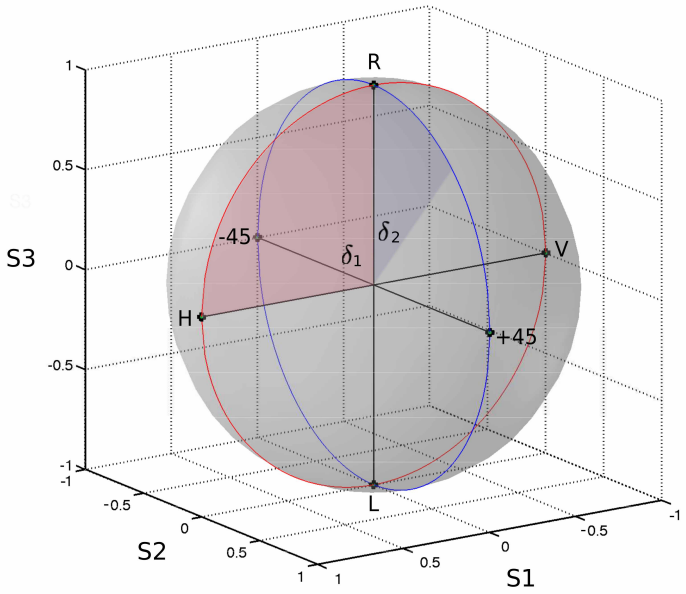

Fig. 3. Illustration of two rotations around two perpendicular axes of the Poincaré sphere. Perpendicular axes on the sphere represent polarization states which have their angle of ellipticity at 45° with respect to each other.

45°. Starting from the point on the Poincaré sphere for horizontal polarization, and rotating by $\pi/2$ clockwise around the 45° axis, the right-circular point on the sphere is reached. This is depicted in Fig. 3, where the rotation is described using retardance δ_1.

A single variable retarder at a fixed orientation can thus introduce a variable rotation on the Poincaré sphere around a fixed axis. In most experimental conditions the initial state of polarization in the laboratory is fixed; therefore, in order to reach any point on the surface of the Poincaré sphere, two linearly independent rotations – equivalent to two retardances – are needed [14, 15]. In other words, two variable retarders are necessary to be able to generate any state of fully polarized light (i.e. to attain full polarization control). As explained before, the orientation of the retardances must be linearly independent on the sphere, such as δ_1 and δ_2 in Fig. 3.

Moreno et al. have recently reported a method to control the polarization of a beam of light using a spatial light modulator [16]. To the best of our knowledge, the analysis and calculations in their publication are useful and accurate; however, it is perhaps unfortunate that they have claimed to attain full polarization control with their method. Their system uses two retarders at a relative angle of 90°. This is equivalent to two rotations around the same axis of the sphere in opposite directions. On the Poincaré sphere, the locus of all the states of polarization that can be produced by their method is a single circular line around the V/H axis. The example that they show in their publication is limited to the narrow blue circular line on Fig. 3. With such a system it is not possible to change the angle of the ellipse of the polarization states produced. Another recent work that, also unfortunately, claims to attain arbitrary space-variant vector beam was published by Chen et al. [17]. Their method effectively uses coherent superposition of a right-circular and a left-circular polarized beam, and it's a very efficient way to produce linearly polarized states. However, the states of polarization that Chen et al. can generate are

#167770 - $15.00 USD Received 1 May 2012; revised 28 May 2012; accepted 29 May 2012; published 8 Jun 2012

also limited to a line on the Poincarè sphere, this time along the equator.

2.1. Complete polarization control: Jones analysis

We will now consider a pair of devices of retardances, δ_1 and δ_2, with their fast axes at a relative angle of 45°. The Jones matrices and vectors used in this section can be found in [18]. We have chosen this formalism in order to later include a term representing the absolute phase in the analysis.

The incident beam used in our analysis was polarized vertically, and thus its normalized Jones vector is:

$$\mathbf{j}_{in} = \begin{bmatrix} 0 \\ 1 \end{bmatrix}. \tag{7}$$

This vertically polarized beam was then incident on a variable retarder with its fast axis at 45°, and then a similar variable retarder with its fast axis at 0°. The general Jones matrix representing a retarder with fast axis at angle θ, and retardance δ is

$$\mathbf{J}_R(\delta,\theta) = \begin{bmatrix} \cos^2\theta + \exp(-i\delta)\sin^2\theta & (1-\exp(-i\delta))\cos\theta\sin\theta \\ (1-\exp(-i\delta))\cos\theta\sin\theta & \exp(-i\delta)\cos^2\theta + \sin^2\theta \end{bmatrix}. \tag{8}$$

This can be calculated using the Jones matrices for a retarder and the two corresponding rotation matrices, in a similar way to the Mueller matrix computation in Eq. (3).

$$\mathbf{J}_R(\delta,\theta) = \mathbf{J}_{rot}(\theta)\cdot\mathbf{J}_{Ret}(\delta)\cdot\mathbf{J}_{rot}(-\theta), \tag{9}$$

where

$$\mathbf{J}_{rot}(\theta) = \begin{bmatrix} \cos\theta & -\sin\theta \\ \sin\theta & \cos\theta \end{bmatrix}, \tag{10}$$

and

$$\mathbf{J}_{Ret}(\delta) = \begin{bmatrix} 1 & 0 \\ 0 & \exp(-i\delta) \end{bmatrix}. \tag{11}$$

From Eq. (8) we calculate the Jones matrix representing the first retardation in the analysis, which has retardance δ_1 and its fast axis at 45°:

$$\mathbf{J}_R(\delta_1,45^\circ) = \frac{1}{2}\begin{bmatrix} 1+\exp(-i\delta_1) & 1-\exp(-i\delta_1) \\ 1-\exp(-i\delta_1) & 1+\exp(-i\delta_1) \end{bmatrix}. \tag{12}$$

Similarly we can calculate the Jones matrix for the second retarder at an angle of 0° and with retardance δ_2:

$$\mathbf{J}_R(\delta_2,0^\circ) = \begin{bmatrix} 1 & 0 \\ 0 & \exp(-i\delta_2) \end{bmatrix}. \tag{13}$$

The Jones vector representing the polarization state of the beam after experiencing the two retardances, $\mathbf{j}_{out}$ is calculated by multiplying $\mathbf{J}_R(\delta_1,45^\circ)$ and $\mathbf{J}_R(\delta_2,0^\circ)$ by $\mathbf{j}_{in}$ as follows

$$\mathbf{j}_{out} = \mathbf{J}_R(\delta_2,0^\circ)\cdot\mathbf{J}_R(\delta_1,45^\circ)\cdot\mathbf{j}_{in}. \tag{14}$$

$\mathbf{j}_{out}$ is, therefore,

$$\mathbf{j}_{out} = \frac{1}{2}\begin{bmatrix} 1 & 0 \\ 0 & \exp(-i\delta_2) \end{bmatrix}\cdot\begin{bmatrix} 1+\exp(-i\delta_1) & 1-\exp(-i\delta_1) \\ 1-\exp(-i\delta_1) & 1+\exp(-i\delta_1) \end{bmatrix}\cdot\begin{bmatrix} 0 \\ 1 \end{bmatrix},$$

$$\mathbf{j}_{out} = \frac{1}{2}\begin{bmatrix} 1-\exp(-i\delta_1) \\ (1+\exp(-i\delta_1))\exp(-i\delta_2) \end{bmatrix}. \tag{15}$$

#167770 - $15.00 USD Received 1 May 2012; revised 28 May 2012; accepted 29 May 2012; published 8 Jun 2012

Note that the horizontal component of $\mathbf{j}_{out}$ depends only on δ_1, and its magnitude can vary continuously between 0 ($\delta_1 = 0$) and 1 ($\delta_1 = \pm\pi$). Likewise, the magnitude of the vertical component depends solely on δ_1, through factor $(1+\exp(-i\delta_1))$. The behavior of this magnitude is of opposite trend to the magnitude of the horizontal component. This shows how the first variable retarder defines how much energy is split between the horizontal and vertical polarization components. Finally, the second variable retardance δ_2 allows us to fine tune the relative phase between the two orthogonal components to define the handedness and final ellipticity of the beam (see Fig. 3).

For simplicity, we have presented the analysis of how to generate truly arbitrary states of polarization using variable retarders on a single pixel. The advantage of using spatial light modulators (e.g. parallel aligned LCoS) is that δ_1 and δ_2 can both vary spatially over the pupil. Therefore, they can be written as $\delta_1(x,y)$ and $\delta_2(x,y)$ (in cartesian coordinates) or $\delta_1(\rho,\phi)$ and $\delta_2(\rho,\phi)$ (in polar coordinates). With such generalization of Eq. (15) the polarization state can be fully and arbitrarily controlled across the initial beam, as will be discussed in the following sections.

3. Experiments

We showed, in the previous section, that two variable retarders oriented at 45° with respect to each other can be used to attain complete polarization control. We now report the experimental system we developed that is capable of implementing this concept. It uses two parallel-aligned nematic spatial light modulators (Boulder Nonlinear Systems XY P512-0532). Each pixel in an SLM acts as an independent variable retarder with fixed fast axis when used at quasi normal incidence (the manufacturer recommends and angle of incidence $< 10°$. The system can generate any polarization state at any pixel on the spatial light modulator. These polarization distributions are focused by a high numerical aperture lens, thus generating fully controllable focused fields.

3.1. Polarization-only control of the distribution in the entrance pupil of a high-NA optical system.

A schematic diagram of the experimental system is shown in Fig. 4. The light source was a linearly polarized 532nm wavelength CW frequency-doubled ND:YAG laser (Melles Griot model 85-GCA-005-100). A calcite polarizer was used to attain high polarization purity and to define the vertical orientation of polarization on the optical bench. The beam was then expanded and spatially filtered. A half waveplate (HWP) with fast axis at 22.5° was used to rotate the polarization of the beam by 45° before the first SLM (SLM1). After the first retardance distribution was applied to the beam using the SLM1, the polarization state was rotated back $-45°$ by the same waveplate after reflection. The net effect of the half waveplate is to virtually rotate the fast axis of the pixels in SLM1, without having to physically rotate the device. This allowed us to match the square geometry of the pixels of the two SLMs (see appendix for a detailed explanation). Lenses L1 and L2 and mirror M were then used to optically conjugate the planes of both SLMs; the magnification of this relay was 1, and had to be accurate to within one pixel (15 μm) so that accurate mapping of pixels between the two SLMs was attained. The configuration results in a relative orientation of 45° between SLM1 and SLM2, which can be used to visit any point on the Poincaré sphere at any pixel across the width of the beam.

After SLM2, another 4f system (lenses L3 and L4) was used to image the desired polarization distribution onto the pupil of a high-NA lens (OBJ) , passing through beam splitter BS. The field at the focus can be tailored dynamically by addressing the retardance distributions on the two SLMs. When a sample (SMP) is placed at the focus the scattered field is then collected, recollimated and imaged (using L5 and L6) onto a CCD camera (D1). The system includes a

#167770 - $15.00 USD Received 1 May 2012; revised 28 May 2012; accepted 29 May 2012; published 8 Jun 2012

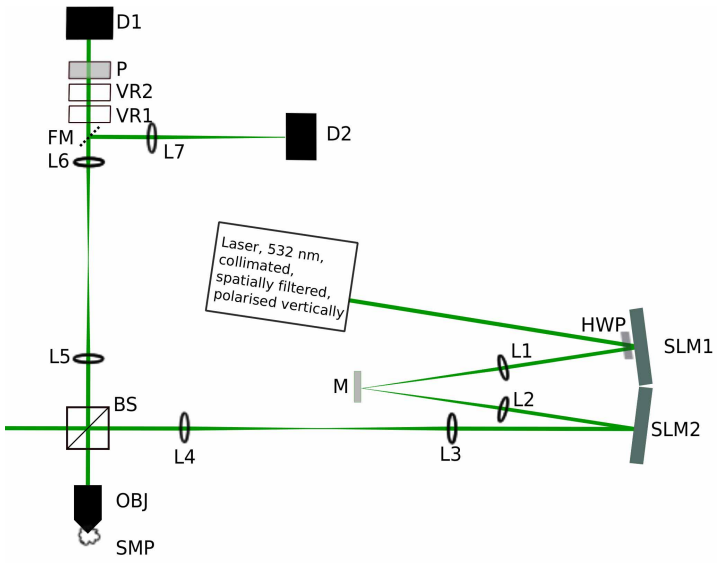

Fig. 4. Schematic diagram of the setup built which can create any polarization state at any point across a laser beam, limited by the pixel size of the spatial light modulator used.

spatial polarization state analyzer, which consists of a pair of liquid crystal variable retarders (VR1 and VR2), again at an angle of 45° with respect to each other, a linear polarizer (P) and camera D1. This system can be used for the technique of vectorial polarimetry, where sub-diffraction limit information is sought from nano-scale samples [19, 20]. The diagram also shows an auxiliary camera (D2) which is accessible by using a flip-in mirror FM. This camera is conjugate to the focal plane of the objective lens, via lens L7, and is useful for the initial positioning of the samples.

A key feature of the experimental system is that the inclusion of the spatial polarization state analyzer (PSA) allowed for the system to be accurately calibrated at every position across the beam. Calibration was performed using the eigenvalue calibration method (ECM) [21, 22], therefore we were able to remove systematic errors in the illumination and the detection separately. For example, beamsplitters like BS in the system can introduce different polarization effects across the beam [23]. We applied the ECM at each position across the beam waist, and effectively removed the systematic errors through the whole system at each and every pixel in the SLMs.

3.2. Example of splitting the focal field into two perpendicularly polarized spots

We now show a simple particular case of a focal field that can be generated by controlling the polarization state in the pupil of a high-NA lens. In this example, the focal field is split into two, spatially separated, perpendicularly polarized spots in the focal plane. This focal field can be produced by generating the polarization distribution shown in Fig. 5 in the pupil of the lens.

To obtain the Stokes vector distribution in Fig. 5 a constant $\pi/2$ retardance was applied to the first SLM and 5 wavelengths of wrapped tilt was used on the second SLM. We calculated the resulting focal field using McCutchen's method [24,25], which is a Fourier-transform based method to implement vectorial diffraction theory. This method greatly simplifies and speeds up the calculation of tightly focused fields resulting from spatially variant polarization distributions [26, 27]. The irradiance of the focal field resulting from this polarization state distribution is shown in Fig. 6, both theoretically calculated with NA $= 0.95$ and from experimental detec-

#167770 - $15.00 USD Received 1 May 2012; revised 28 May 2012; accepted 29 May 2012; published 8 Jun 2012

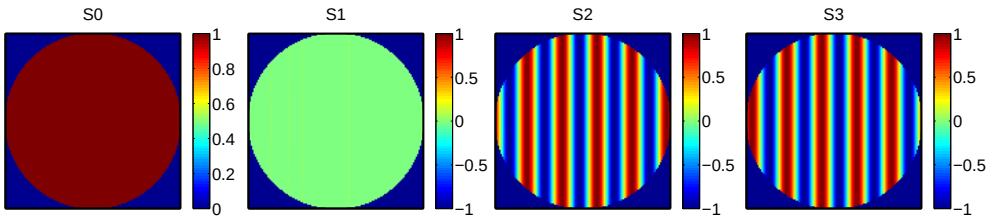

Fig. 5. Stokes vector distribution of the polarization state in the pupil of the high-NA lens which results in two perpendicularly polarized spots in the focal field. A uniform retardance of $\pi/2$ is used on the first SLM, while five wrapped waves of tilt in retardance are applied on the second. The incident beam is uniformly vertically polarized.

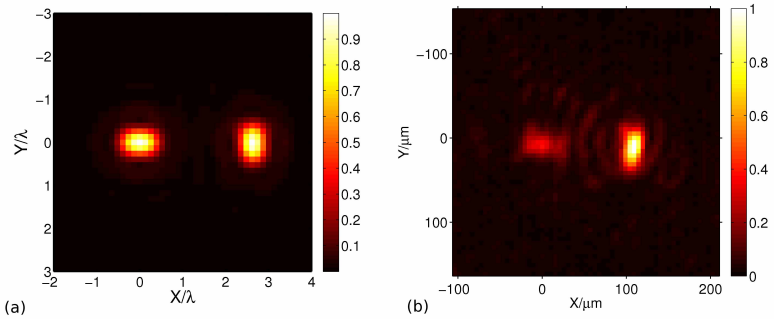

Fig. 6. Theoretical (a) and experimental (b) intensities for the split focal field. The right image was acquired using the auxiliary camera (D2 in Fig. 4), after re-imaging the field at low-NA.

tion after re-imaging the focus field on a CCD.

The two bright spots in Fig. 6 have orthogonal polarizations, and the separation between them depends on the magnitude and the direction of the retardance tilt applied to the second SLM. The spots show the typical elongation of the focal spot along the direction of linear polarization when focusing at high NA [1]. The theoretical components of the focused field at the focal plane are shown in in Fig. 7.

The experimental results in Fig. 6, and later Fig. 9, were obtained by focusing the polarization distribution depicted in Fig. 5, using a high-NA objective lens (OBJ in Fig. 4), onto a microscope slide. The objective used with our system was an Olympus UPLSAPO 100x, NA = 1.4 in n = 1.518 immersion oil. The focal field was reflected off the air-glass interface at the focus of the objective, and re-imaged at low-NA (approximately 0.02) onto the plane of detection of the auxiliary camera. This plane was conjugate to the focal plane of OBJ, and a high-magnification image of the focal plane could be obtained there. The separation of the focal spots was detectable at this plane as it is due to differences in the directions of propagation of perpendicular polarization states, which is not a high-NA effect. The nominal magnification between the field at the tight focus and the image on camera D2 was on the order of 100×, therefore the separation between the measured spots was on the order of 100 μm, when the wavelength of the focused laser light was 0.532 μm.

We note that in this example the polarization state at each position on the pupil is resolved into vertical and horizontal components, therefore they have equal magnitude at all points. The

#167770 - $15.00 USD Received 1 May 2012; revised 28 May 2012; accepted 29 May 2012; published 8 Jun 2012

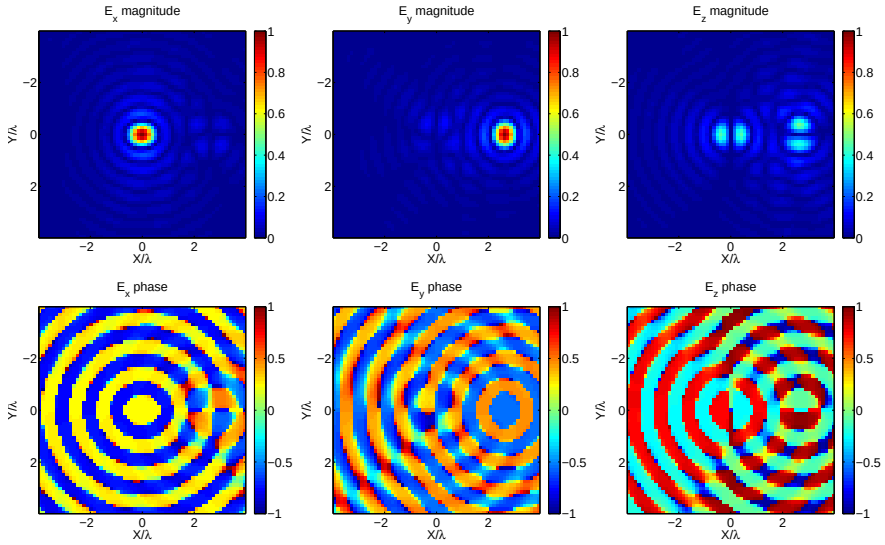

Fig. 7. Magnitude and phase of the three components of the electric field of the intensity distribution in Fig. 6(a).

combination of retardances on both SLMs converts the field in the pupil into a coherent superposition of an *x*-polarized incident beam propagating parallel to the optical axis of the objective lens, and a *y*-polarized incident beam with direction of propagation at an angle with respect to the optical axis. This angle depends on the number of waves of tilt in retardance and the direction of the tilt. This difference in the direction of propagation of the perpendicularly polarized incident fields results in the spatial separation of the perpendicularly polarized focused fields. This is a highly controllable superposition of orthogonally polarized spots that could be used as a dynamic optical probe by adjusting the retardance tilt applied to the SLMs.

The polarization distribution in this example was constant along the y-axis of the pupil, and varied along the x-axis of the pupil (see Fig. 5). The polarization modulation along the x-axis corresponds to 5 full rotations on the Poincaré sphere, around the V-H axis, passing through linear at $+45^{\circ}$, right circular, linear at -45°, left circular, and polarizations states in between. The locus on the Poincaré sphere that these states of polarization can visit is a single circular line around the V/H axis, just as in the method reported by Moreno et al. [16].

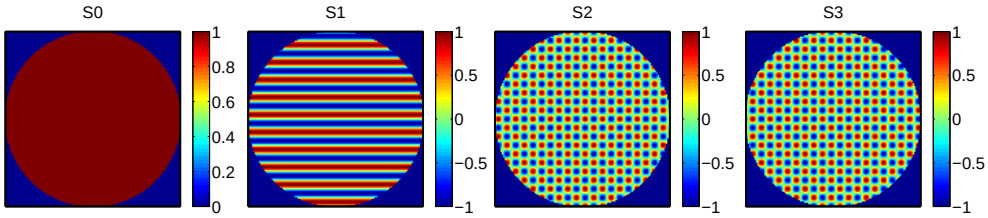

Fig. 8. Polarization state in the pupil of the high-NA lens which results in four perpendicularly polarized spots in the focal field. Ten wrapped waves of tilt in retardance are applied by each SLM. These tilts are perpendicular to each other.

In this first example, the retardance on the first SLM was kept constant, which could be per-

#167770 - $15.00 USD Received 1 May 2012; revised 28 May 2012; accepted 29 May 2012; published 8 Jun 2012

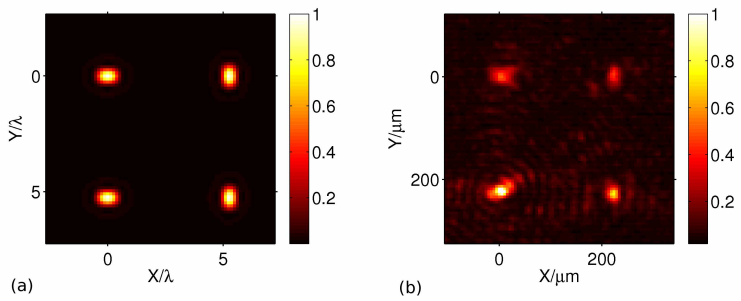

Fig. 9. Irradiance of the focused field, theoretically calculated using McCutchen's method (a), and experimentally measurement after re-imaging the field at high–magnification (b).

formed with a homogeneous retarder. Strictly speaking only one pass on an SLMs is necessary to generate that distribution, and we emphasize that full polarization control is therefore not shown by this example. Nevertheless, the strong dependence of the field at the focus of a high-NA lens on the pupil polarization state is evident, and we will now give another similar example which uses the full capabilities of the spatial polarization state generator.

In this further example, tilts in retardance are applied to both SLMs in perpendicular directions. The Stokes parameters of the resulting polarization distribution are shown in Fig. 8. Focusing this polarization distribution results in a field at the focus with four bright spots. The theoretical and experimentally measured intensity of the focused field are shown in Fig. 9. The magnitude and phase of the components of the electric field at the focus are shown in Fig. 10. Theoretical calculations were again obtained using McCutchen's method with a numerical aperture of 0.95.

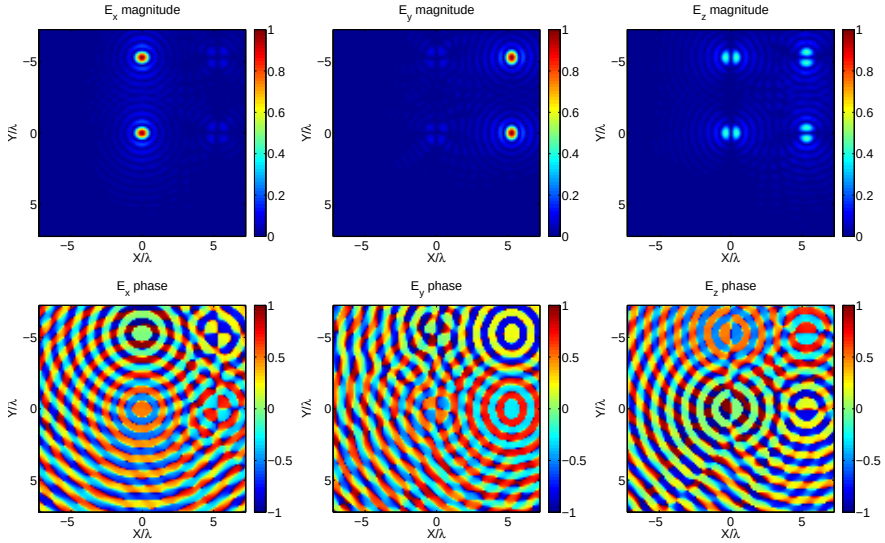

Fig. 10. Magnitude and phase of the components of the field in the focus using the polarization state shown in Fig. 8.

#167770 - $15.00 USD Received 1 May 2012; revised 28 May 2012; accepted 29 May 2012; published 8 Jun 2012

4. Full spatial polarization control with additional phase wavefront control

Radial and azimuthal polarization, the two orthogonal components of cylindrical beams [28], are two examples of spatially varying polarization distributions. When they are decomposed in cartesian coordinates they also possess a vortex in their absolute phase. We discussed above the difference between a radially polarized beam with and without phase control (see again Fig. 1). In practice, it is not possible to produce cylindrical beams with polarization only control, unless the orientation of the fast axis can be changed spatially across the pupil plane, as in [29]. Commercial spatial light modulators have a fixed orientation of their fast/slow axes, hence a further phase control step is needed to produce beams with radial or azimuthal polarization components.

4.1. Modification to setup to incorporate absolute phase control

Recalling Eq. (15), we note that two retardances can be used to change a fixed input polarization state into any other polarization state, which is equivalent to two perpendicular rotations on the Poincaré sphere. These retardances can vary spatially across the waist of the beam, for example, if spatial light modulators are used to control the retardances. If we now introduce a pure phase term $\phi(x,y)$ that can also vary spatially across the beam, Eq. (15) becomes

$$\mathbf{j}_{out}(x,y) = \frac{\exp(-i\phi(x,y))}{2}\begin{bmatrix} 1-\exp(-i\delta_1(x,y)) \\ (1+\exp(-i\delta_1(x,y)))\exp(-i\delta_2(x,y)) \end{bmatrix}. \tag{16}$$

In general, $\phi(x,y)$ will correspond to a vortex in absolute phase for a cylindrical beam.

The experimental setup needed to incorporate this absolute phase control, along with the two SLM passes for full polarization control is shown in Fig. 11. In this version of the setup, the phase control is performed before the polarization modulation, thus the half wave plate (HWP) is now placed in front of the second SLM (SLM2). The incident beam on the first SLM is vertically polarized and aligned with the slow axis of the SLM. Since the slow axis is the active axis, this step changes only the absolute phase of the beam according to the pattern applied to the part of the SLM on which the beam is incident. This is exactly how an SLM is operated in adaptive optics and wavefront control, which is a feature of the system that can be further exploited to compensate for sample or system induced aberrations. The subsequent two SLM passes act as described in Fig. 4 where the half waveplate at 22.5° is placed between the second two passes to give rise to the relative angle of 45° between these two retardances.

4.2. Focusing of a cylindrical polarization state defined using Zernike polynomials

We now introduce a polarization distribution that makes use of pure phase control and full polarization control in terms of cylindrical beams. We use a polar coordinate system, decomposing the field into radial and azimuthal components, $\vec{E}_p$ and $\vec{E}_s$ respectively. This coordinate system inherently includes the vortex in phase which is a defining characteristic of cylindrical beams, as it will be seen later. We defined the distribution by making the retardance between the radial and azimuthal components a Zernike polynomial [30]. We will then show a calculated focused field, which can be produced using the setup described in Fig. 11. A vortex in absolute phase is applied to the beam on the first pass, while the second and third passes are used to generate the spatially variant polarization distribution.

The polarization state in the pupil of the high-NA objective lens is shown in Fig. 12. The figure shows the field in small local polar coordinate systems, or in other words in radial and azimuthal components, $\vec{E}_p$ and $\vec{E}_s$, respectively. The relative phase difference (retardance) between $\vec{E}_p$ and $\vec{E}_s$, $\delta = \delta_p - \delta_s$, is a distribution given by Zernike polynomial Z_3^3. In the areas of the pupil where the retardance is zero linearly polarized light is present, however the direction

#167770 - $15.00 USD Received 1 May 2012; revised 28 May 2012; accepted 29 May 2012; published 8 Jun 2012

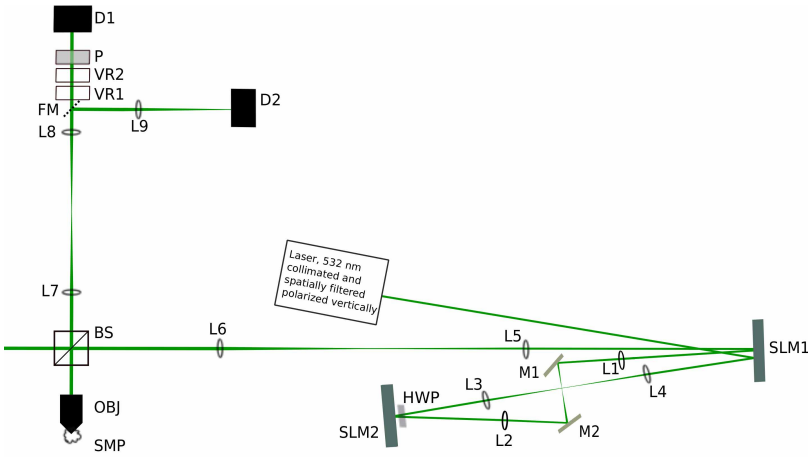

Fig. 11. Modified setup which includes both absolute phase and complete polarization control spatially over the pupil distribution.

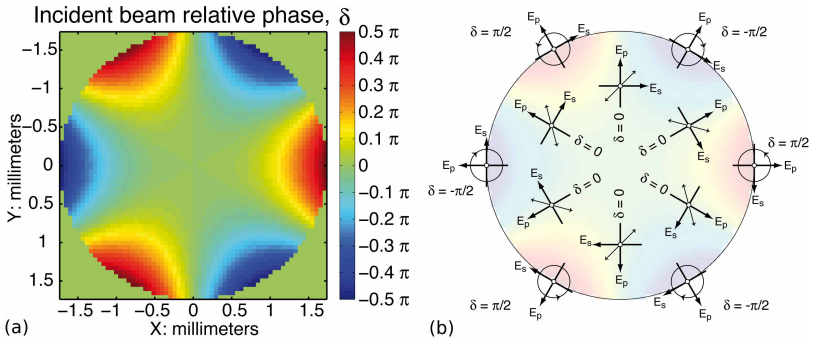

Fig. 12. Retardance of the pupil polarization distribution (a), defined using a Z_3^3 Zernike polynomial with amplitude $\pi/2$ (in the Born and Wolf normalization [31]). A schematic diagram of the local coordinate systems and polarization states is shown in (b).

of polarization changes with azimuthal position such that the radial and azimuthal components have equal magnitude everywhere. Moving towards the edge of the pupil, the retardance tends to increase in some regions (red and blue lobes), hence the ellipticity also increases. Note that this field has a singularity in the middle of the pupil (on the optical axis of the propagating beam), typical of vortex beams.

We used McCutchen's method to calculate the field that can be produced by focusing the polarization distribution in Fig. 12. The magnitude and phase of the components of this field are shown in Fig. 13. A triangular shape with 3 lobes is apparent in both the radial and azimuthal components of this focal field. The key feature of this field is that the state of polarization varies rapidly through the focal region. For this reason we anticipate that this field will be useful for the technique of vectorial polarimetry [19], to detect asymmetries in nano-scale samples, for example by rotating the triangular lobe-shaped focused field around an asymmetric sample. Possible applications of this technique would be in defect detection and optical storage. Other geometries of focal field can be generated using further Zernike patterns, producing many different symmetries of focal field. It is anticipated that this property could be used to increase resolution in an imaging system by tailoring the focal field to the specimen under consideration.

#167770 - $15.00 USD Received 1 May 2012; revised 28 May 2012; accepted 29 May 2012; published 8 Jun 2012

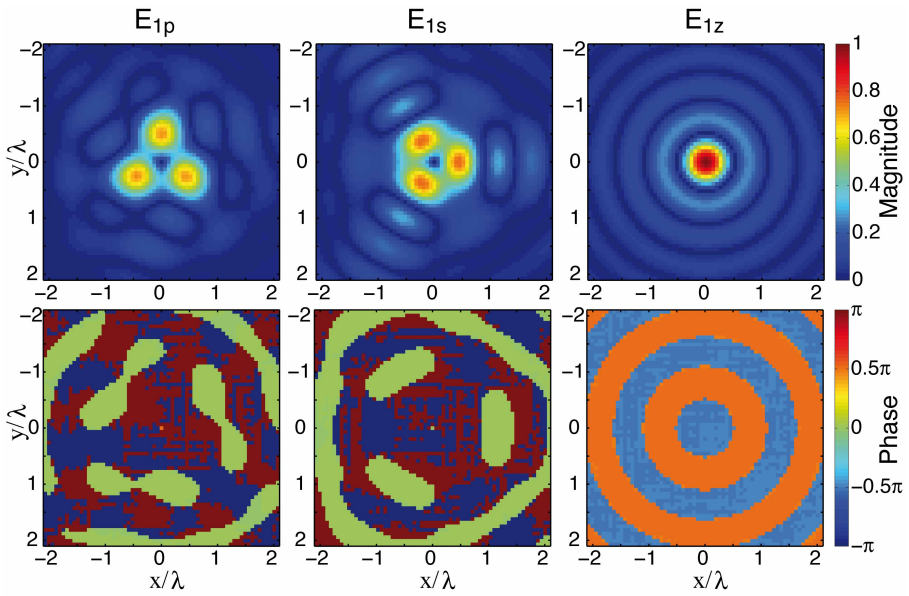

Fig. 13. The magnitude and phase of the focal field components shown in a polar coordinate system. Note the triangular symmetry of the $\vec{E}_p$ and $\vec{E}_s$ components.

5. Conclusion

In this work, we have shown, using Jones analysis, that complete polarization control requires two linearly independent retardations on the Poincaré sphere. These retardations are easily visualized as two rotations on the surface of the sphere. The analysis presented in this paper is valid when a starting point on the sphere is constant, and also when retarders with fixed orientations of fast axis are used. We also presented a system capable of implementing the concepts of complete spatial polarization control and a modified version of the system which controls, again spatially across the waist of a beam, the absolute phase of the beam.

The field at the focus of a high numerical aperture lens depends strongly on the polarization and phase distribution in the pupil. In the case of tight focusing, vectorial diffraction, which takes into account the polarization of the light in the pupil, must be used to calculate the focused field. McCutchen's method, which uses a Fourier approximation to the vectorial diffraction integrals, has been used in this paper due to fast calculation times, and the ease of defining spatially variant polarization and phase distributions as the input parameters.

The shape of the focal field can be changed into useful shapes that may be useful for specific applications. A number of potentially useful fields have been described in this paper, including fields where the energy is separated into orthogonally polarized and spatially separated spots. This could amount to a differential polarization probe. Also, a focal field, calculated from a pupil distribution which was defined by Zernike polynomials, was shown, the asymmetry of which could be used to detect further asymmetries or defects in nano-scale samples. This work opens up many possibilities of tailoring the focal field of a high-NA lens to the specimen under consideration or the application desired.

6. Appendix

We explain the effect of using the half waveplate HWP in the experimental systems using multiple applications of Eq. (9). The sequence of optical components in this part of the system

#167770 - $15.00 USD Received 1 May 2012; revised 28 May 2012; accepted 29 May 2012; published 8 Jun 2012

starts with the half waveplate in the forward direction $\mathbf{J}_{HWP^+} = \mathbf{J}_R(\pi, 22.5^\circ)$, the retardance introduced by the SLM in the forward direction $\mathbf{J}_{SLM^+} = \mathbf{J}_R(\delta_1/2, 0)$, and a reflection by an ideal mirror on the backplane of the SLM $\mathbf{J}_{Mirror}$. Then the SLM introduces a retardance in the backward direction $\mathbf{J}_{SLM^-} = \mathbf{J}_R(\delta_1/2, 0)$ and finally the beam goes through the half waveplate again $\mathbf{J}_{HWP^-} = \mathbf{J}_R(\pi, -22.5^\circ)$ also in the backward direction. The state of polarization after this sequence is

$$\mathbf{j}_{SLM_1} = \mathbf{J}_{HWP^-} \cdot \mathbf{J}_{SLM^-} \cdot \mathbf{J}_{Mirror} \cdot \mathbf{J}_{SLM^+} \cdot \mathbf{J}_{HWP^+} \cdot \mathbf{j}_{in}. \tag{17}$$

Or, explicitly

$$\begin{aligned} \mathbf{j}_{SLM_1} = & \mathbf{J}_{rot}(-22.5^\circ) \cdot \mathbf{J}_{Ret}(\pi) \cdot \mathbf{J}_{rot}(22.5^\circ) \cdot \mathbf{J}_{Ret}(\delta_1/2) \cdot \\ & \mathbf{J}_{Mirror} \cdot \mathbf{J}_{Ret}(\delta_1/2) \mathbf{J}_{rot}(22.5^\circ) \cdot \mathbf{J}_{Ret}(\pi) \cdot \mathbf{J}_{rot}(-22.5^\circ) \cdot \mathbf{j}_{in}. \end{aligned} \tag{18}$$

Using simple matrix algebra we can see that the following identities hold:

$$\mathbf{J}_{Ret}(\pi) \cdot \mathbf{J}_{rot}(\theta) = \mathbf{J}_{rot}(-\theta) \cdot \mathbf{J}_{Ret}(\pi), \tag{19}$$

$$\mathbf{J}_{Ret}(\alpha) \cdot \mathbf{J}_{Mirror} = \mathbf{J}_{Mirror} \cdot \mathbf{J}_{Ret}(\alpha), \tag{20}$$

$$\mathbf{J}_{Ret}(\alpha) \cdot \mathbf{J}_{Ret}(\beta) = \mathbf{J}_{Ret}(\beta) \cdot \mathbf{J}_{Ret}(\alpha) = \mathbf{J}_{Ret}(\alpha + \beta). \tag{21}$$

And with these it is straightforward to show that

$$\mathbf{j}_{SLM_1} = \mathbf{J}_{Mirror} \cdot \mathbf{J}_{rot}(45^\circ) \cdot \mathbf{J}_{Ret}(\delta_1) \cdot \mathbf{J}_{rot}(-45^\circ) \cdot \mathbf{j}_{in}, \tag{22}$$

which explains the virtual rotation of the pixels in the SLM by 45°.

Acknowledgment

This research was support by Science Foundation Ireland under Grant No. 07/IN.1/I906.

#167770 - $15.00 USD Received 1 May 2012; revised 28 May 2012; accepted 29 May 2012; published 8 Jun 2012